Molecular Therapy
Nucleic Acids
Original Article

Oligo-PROTAC strategy for cell-selective and targeted degradation of activated STAT3

Jeremy Hall,[1,5] Zhuoran Zhang,[1,5] Supriyo Bhattacharya,[2] Dongfang Wang,[1] Marice Alcantara,[1] Yong Liang,[3] Piotr Swiderski,[3] Stephen Forman,[4] Larry Kwak,[4] Nagarajan Vaidehi,[2] and Marcin Kortylewski[1]

[1]Department of Immuno-Oncology, Beckman Research Institute, City of Hope, Duarte, CA 91010, USA; [2]Department of Computational and Quantitative Medicine, Beckman Research Institute, City of Hope, Duarte, CA 91010, USA; [3]DNA/RNA Synthesis Core Facility, Beckman Research Institute, City of Hope, Duarte, CA 91010, USA; [4]Department of Hematology & Hematopoietic Cell Transplantation, Beckman Research Institute, City of Hope, Duarte, CA 91010, USA

Decoy oligodeoxynucleotides (ODNs) allow targeting undruggable transcription factors, such as STAT3, but their limited potency and lack of delivery methods hampered translation. To overcome these challenges, we conjugated a STAT3-specific decoy to thalidomide, a ligand to cereblon in E3 ubiquitin ligase complex, to generate a proteolysis-targeting chimera (STAT3D^{PROTAC}). STAT3D^{PROTAC} downregulated STAT3 in target cells, but not STAT1 or STAT5. Computational modeling of the STAT3D^{PROTAC} ternary complex predicted two surface lysines, K601 and K626, in STAT3 as potential ubiquitination sites. Accordingly, K601/K626 point mutations in STAT3, as well as proteasome inhibition or cereblon deletion, alleviated STAT3D^{PROTAC} effect. Next, we conjugated STAT3D^{PROTAC} to a CpG oligonucleotide targeting Toll-like receptor 9 (TLR9) to generate myeloid/B cell-selective C-STAT3D^{PROTAC}. Naked C-STAT3D^{PROTAC} was spontaneously internalized by TLR9^{+} myeloid cells, B cells, and human and mouse lymphoma cells but not by T cells. C-STAT3D^{PROTAC} effectively decreased STAT3 protein levels and also STAT3-regulated target genes critical for lymphoma cell proliferation and/or survival (*BCL2L1*, *CCND2*, and *MYC*). Finally, local C-STAT3D^{PROTAC} administration to human Ly3 lymphoma-bearing mice triggered tumor regression, while control C-STAT3D and C-SCR treatments had limited effects. Our results underscore the feasibility of using a PROTAC strategy for cell-selective, decoy oligonucleotide-based STAT3 targeting of and potentially other tumorigenic transcription factors for cancer therapy.

INTRODUCTION

Signal transducer and activator of transcription 3 (STAT3) is a transcription factor (TF) and prominent oncogene responsible for tumorigenesis and immune evasion associated with poor prognosis in a variety of human cancers.[1–3] STAT3 is activated by a variety of upstream cytokine and growth factor receptor-associated tyrosine kinases, such as Janus kinase (JAK1, JAK2) or oncogenic Src and Abl kinases, resulting in the formation of homo- or hetero-dimers, which are then translocated to the nucleus to initiate downstream gene expression.[1,4] Abnormal STAT3 signaling in tumor and tumor-associated myeloid cells has been shown to affect the regulation of genes relevant to such cellular functions as angiogenesis, cell signaling, immunosuppression, inflammation, proliferation, and metastasis. As a result, STAT3 has emerged as a distinctly unique and attractive target in cancer therapy.[2,5,6] However, because of the lack of kinase domain and largely planar surface area for protein-protein interactions, TFs such as STAT3 are challenging pharmacologic targets.[5,7,8] Synthetic oligonucleotides such as STAT3 decoy DNA or antisense oligonucleotides (ASOs) have shown promise in clinical trials and were well tolerated in patients.[9–11] However, except for hepatocyte targeting, lack of cell-selective delivery strategies remains a key challenge for the majority of oligonucleotide therapeutics.[12] Broad and non-cell-selective STAT3 inhibition is likely to result in conflicting effects on the immune cell network, thereby limiting the long-term antitumor immune responses. This is due partly to STAT3 role in the expansion of cytotoxic CD8 T cells in cancer patients[13] and in the development and maintenance of memory T cells.[14] To overcome these limitations, we previously developed a strategy to deliver oligonucleotide-based STAT3 inhibitors, such as small interfering RNA (siRNA), ASO, or decoy oligodeoxynucleotides (ODNs), specifically into tumor-associated myeloid cells, B cells, and some cancer cells.[15] Conjugation of STAT3 decoy to Toll-like receptor 9 (TLR9) ligands, CpG oligonucleotides, facilitated targeting of TLR9^{+} immune and cancer cells, prompting immune activation and antitumor responses.[15] CpG-STAT3 decoy conjugate (CpG-STAT3D) was effective in delivering decoy molecules into human and mouse dendritic cells (DCs), macrophages, and myeloid-derived suppressor cells (MDSCs) and also into myeloid leukemia or B cell lymphoma cells in mice.[16,17] More recently, we successfully adopted a CpG decoy strategy for targeting canonical and non-canonical NF-κB signaling specifically in human and mouse B cell lymphoma cells *in vivo*.[18] The antitumor efficacy of both STAT3- and NF-κB-specific CpG decoy strategies resulted mainly from the induction of myeloid or B cell differentiation driving the activation of antitumor immune

Received 3 August 2023; accepted 31 January 2024;
https://doi.org/10.1016/j.omtn.2024.102137.

[5]These authors contributed equally

Correspondence: Marcin Kortylewski, Department of Immuno-Oncology, Beckman Research Institute, City of Hope, Duarte, CA 91010, USA.
E-mail: mkortylewski@coh.org

This is an open access article under the CC BY-NC-ND license (http://creativecommons.org/licenses/by-nc-nd/4.0/).

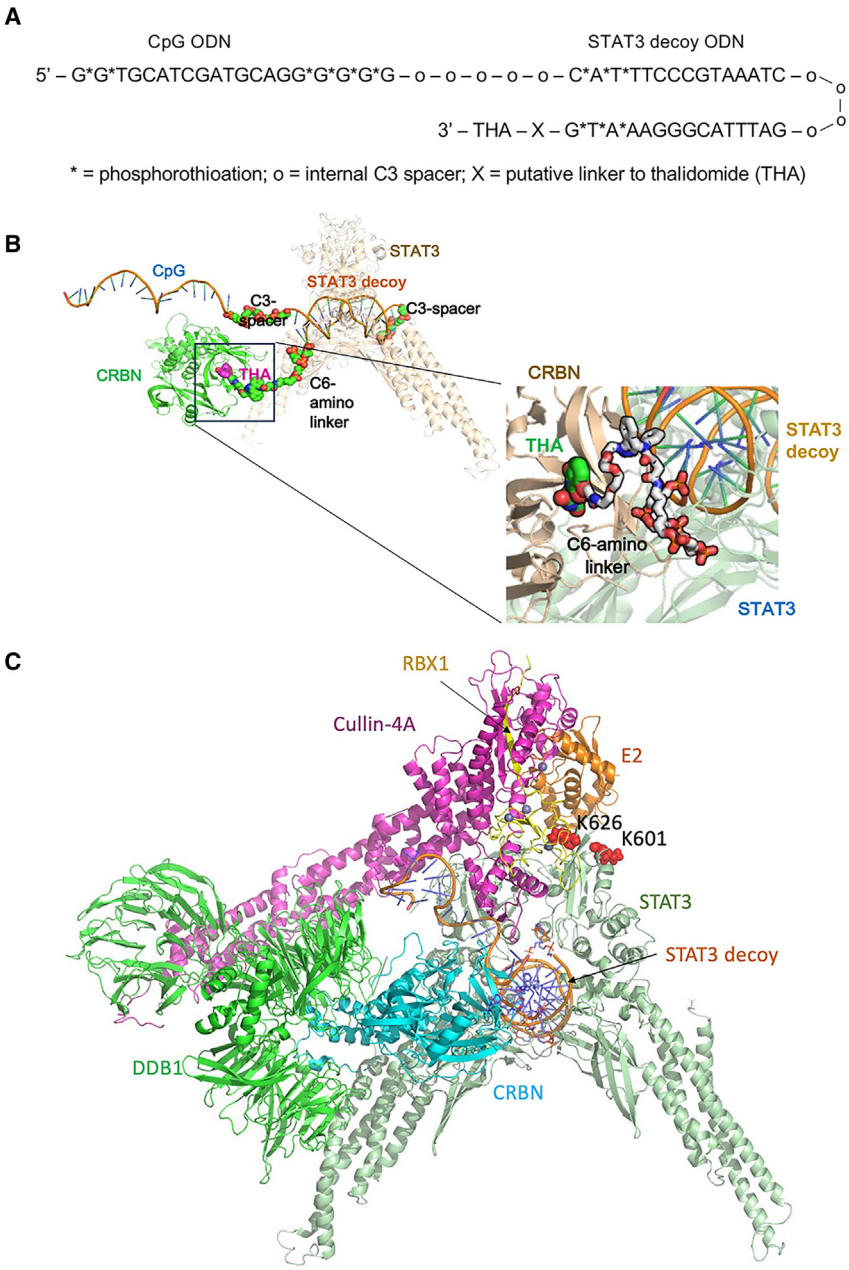

Figure 1. Molecular modeling of the ternary complex involving STAT3, the oligo-PROTAC, and the E3 ligase complex in solution

(A) The tentative sequence of oligo-PROTAC conjugate (C-STAT3DPROTAC) combining a hairpin CpG-STAT3 decoy molecule with thalidomide as an E3 ligase targeting moiety. (B and C) Computational molecular dynamics simulations of C-STAT3DPROTAC oligonucleotide interaction with an activated STAT3 protein dimer and the E3 ligase complex displayed using Maestro software. (B) Modeling of the thalidomide and cereblon (CRBN) binding site. (C) Structural model of the ternary complex of C-STAT3DPROTAC together with the bound STAT3 protein and the multicomponent E3 ligase complex.

responses.[17,18] However, the direct cytotoxic effects of decoy molecules against rapidly proliferating cancer cells may have been limited by the reversibility of dose-dependent target inhibition.

Over the past 20 years, proteolysis-targeting chimeras (PROTACs) have emerged as a unique modality to target and degrade an intracellular protein of interest (POI) by using E3 ubiquitin ligases for proteasomal degradation.[19,20] PROTACs typically consist of two small molecules, one that recruits the E3 ligase and another that binds to the POI, connected by a linker molecule.[21] The chemical nature and length of the linker are critical factors in defining an effective interaction between the POI and the E3 complex.[22] As PROTACs do not require high affinity binding to the target, they have potential to extend their inhibitory effect to yet "undruggable" TFs and also yield target specificity.[20] In addition, the stability of PROTACs enables recycling of the same molecule to degrade multiple copies of the target protein in a catalytical process, maximizing their potency.[23] PROTAC designs commonly use thalidomide or lenalidomide, related immunomodulatory drugs that can recruit cereblon (CRBN) protein within the E3 ligase complex.[21,24] Such small-molecule PROTACs demonstrated ability to degrade multiple oncoproteins, including AKT, BRD4, and EGFR but only lately were tested for STAT3 targeting.[20,24,25] Recently developed small molecule SD-36 is a lenalidomide-based STAT3 degrader. SD-36 showed activity against acute myeloid leukemia (AML) and large-cell lymphoma cells *in vitro* and in immunodeficient mice but lacks cell selectivity, which is critical for generating effective antitumor immune responses.[25,26]

Here, we outline a rational STAT3 oligo-PROTAC design on the basis of a structural modeling of interactions between a decoy-bound protein target and E3 ligase complex. Coupled with TLR9-directed delivery strategy, our approach allows cell-targeted and STAT3-selective degradation to improve antitumor efficacy and safety.

RESULTS

Oligo-PROTAC design for targeted degradation of STAT3

In order to generate a STAT3 proteolysis-targeting chimeric ODN, we equipped CpG-STAT3 decoy with thalidomide molecule attached using a propanediol linker to the 3′ end of the double-stranded decoy hairpin (Figures 1A and S1).[16,17,27] Thalidomide, as a ligand for CRBN protein, could facilitate interaction between an E3 ligase

complex and the STAT3 protein dimer bound to the decoy conjugate. Although there are a few crystal structures of small-molecule PROTAC-mediated complex of CRBN with target proteins, these PROTACs are smaller and different in chemistry than oligo-PROTACs, making them less relevant to current modeling. To validate this hypothesis, we performed computational analysis combining *in silico* modeling and molecular dynamics (MD) simulations (see materials and methods for details). To generate the ternary complex structural model, we first placed STAT3 protein dimer bound to decoy ODN-thalidomide together with thalidomide-bound CRBN using rigid body translation and rotation of CRBN in Maestro software. The rest of the linker and CpG part of the ODN were then added manually, generating the initial structure of the oligo-PROTAC complexed STAT3 and CRBN (Figure 1B). We then subjected this CRBN-associated STAT3 structure to MD simulations in an implicit water environment, as it allows accelerated dynamics and achieve fast diffusion of CRBN, resulting in the binding of STAT3 (Figure S2A). We performed three MD simulation runs with different starting velocities, each 100 ns long, which led to the CRBN-bound STAT3 structure, as evidenced by the gradual decrease in the center-of-mass distance between CRBN and STAT3, stabilizing around 50–55 Å (Figure S2B; Video S1). To analyze the effect of the PROTAC on the stability of the ternary complex, we calculated the binding free energies of STAT3 binding to CRBN with and without the oligo-PROTAC (Figure S2C). The binding free energy between STAT3 and CRBN calculated from all the three MD runs, was significantly better with the oligo-PROTAC rather than without, demonstrating that the oligo-PROTAC leads to enhanced binding between CRBN and STAT3. As shown in Figure 1B, the 3′ end-located thalidomide can bind to the tri-Trp pocket of CRBN without any likely interference from the 5′ CpG part of the oligonucleotide.[28,29]

To predict the proximity of the lysines that get ubiquitinated in STAT3 by E3-E2 ligase complex, we generated a structural model of the STAT3-PROTAC-E3 ligase supramolecular complex (please see methods section; Figure S2). The last frames from the three MD runs were used to model the complete E3/oligo-PROTAC/STAT3 ligase supramolecular complex structure. We first modeled the E3 ligase using two different crystal structures either containing CRBN, DDB1, Cullin4A, and RBX1 without E2 subunit or including E2 bound to RNF4, a RING domain protein analogous to RBX1. The two structures were combined by aligning the RBX1 moiety of the first structure with RNF4 of the second structure, followed by the deletion of RNF4, to obtain the complete E3 ligase structure (Figure S2D). Finally, the E3 ligase structure was aligned with the MD simulation-derived CRBN/oligo-PROTAC/STAT3 structure via their respective CRBN moieties, resulting in a complete E3 ligase/oligo-PROTAC/STAT3 structure (Figures 1C and S2E). Out of the three structural models generated, we selected the one with the least amount of clashes between STAT3 and E3 ligase as our final model (see materials and methods for more details). Our structural model of the larger complex provided support for a potential interaction of the catalytic domain of E2 subunit with lysine residues within the SH2 domain in the C terminus of STAT3 protein as discussed later.

On the basis of these modeling results, we first synthesized a thalidomide-conjugated STAT3 decoy ODN alone (STAT3DPROTAC) without targeting CpG domain (Figure 2A). To assess the relationship between linker length and the STAT3DPROTAC activity, we compared three conjugate designs either directly conjugated to thalidomide (without a linker) or connected via a single or three spacer units. The activity of STAT3DPROTAC variants was assessed in mouse DC2.4 DCs with constitutively activated STAT3 (DC2.4-S3C).[30] Consistently with our computational model, the single spacer linker resulted in the maximal reduction of STAT3 protein levels in target mouse DC2.4-S3C DCs (Figure 2B). The linker length did not affect selectivity of STAT3 targeting (Figure S3A). Next, we performed competition experiments to verify that the inhibitory effect of STAT3DPROTAC relied on both STAT3 decoy (for POI targeting) and thalidomide (for E3 ligase recruitment) parts of the conjugate. All samples were transfected with an equimolar concentration of STAT3DPROTAC followed by increasing concentrations of either the unconjugated STAT3D (Figure 2C) or free thalidomide (Figure 2D), while a scrambled ODN (SCR) served as a negative control. The concurrent treatments with the unconjugated STAT3D or free thalidomide almost completely abrogated inhibition at the target pSTAT3 and total protein levels by STAT3DPROTAC. To initially demonstrate a proof of concept, we transfected DC2.4-S3C (Figure 2E) and mouse A20 lymphoma cells (Figure 2F) with increasing equimolar concentrations of either STAT3D or STAT3DPROTAC. One day later, STAT3DPROTAC reduced activated and total STAT3 levels by more than 80% in DC2.4-S3C cells (at 200 nM) and A20 cells (at 400 nM) compared with STAT3D, which was 2- to 3-fold less potent in reducing pSTAT3 and total STAT3 levels (Figures 2E and 2F, respectively). Finally, we evaluated the specificity of STAT3DPROTAC inhibitory effect. As shown in Figure 2G, STAT3DPROTAC effectively reduced STAT3 protein levels without affecting the closely related STAT1 and STAT5 TFs in the target DC2.4-S3C cells. Thus, STAT3DPROTAC oligonucleotide is shown to inhibit STAT3 signaling with high molecular selectivity.

STAT3D^{PROTAC} induces CRBN-mediated proteasomal degradation of STAT3

We next verified whether STAT3DPROTAC-induced STAT3 inhibition is in fact dependent of proteolytic degradation of the target protein rather than its sequestration as in case of the original STAT3D molecule. As shown in Figure 3A, blocking 26S proteosome function using MG132 peptide inhibitor completely abrogated STAT3DPROTAC effect and stabilized levels of activated and total STAT3 in DC2.4-S3C cells. To elucidate the mechanism further, we assessed the contribution of CRBN toward proteolytic STAT3 degradation. We compared the effect of STAT3DPROTAC in CRBN-positive (Figures 3B and 3C) and in CRBN-deficient (Figures 3B and 3D) DC2.4-S3C cells. As expected, the CRBN-negative target cells completely lost sensitivity to STAT3DPROTAC compared with CRBN-positive cells. This result confirms that CRBN recruitment by thalidomide equipped decoy ODN is critical for the inhibitory effect of STAT3DPROTAC. Our molecular modeling of the ternary complex involving STAT3,

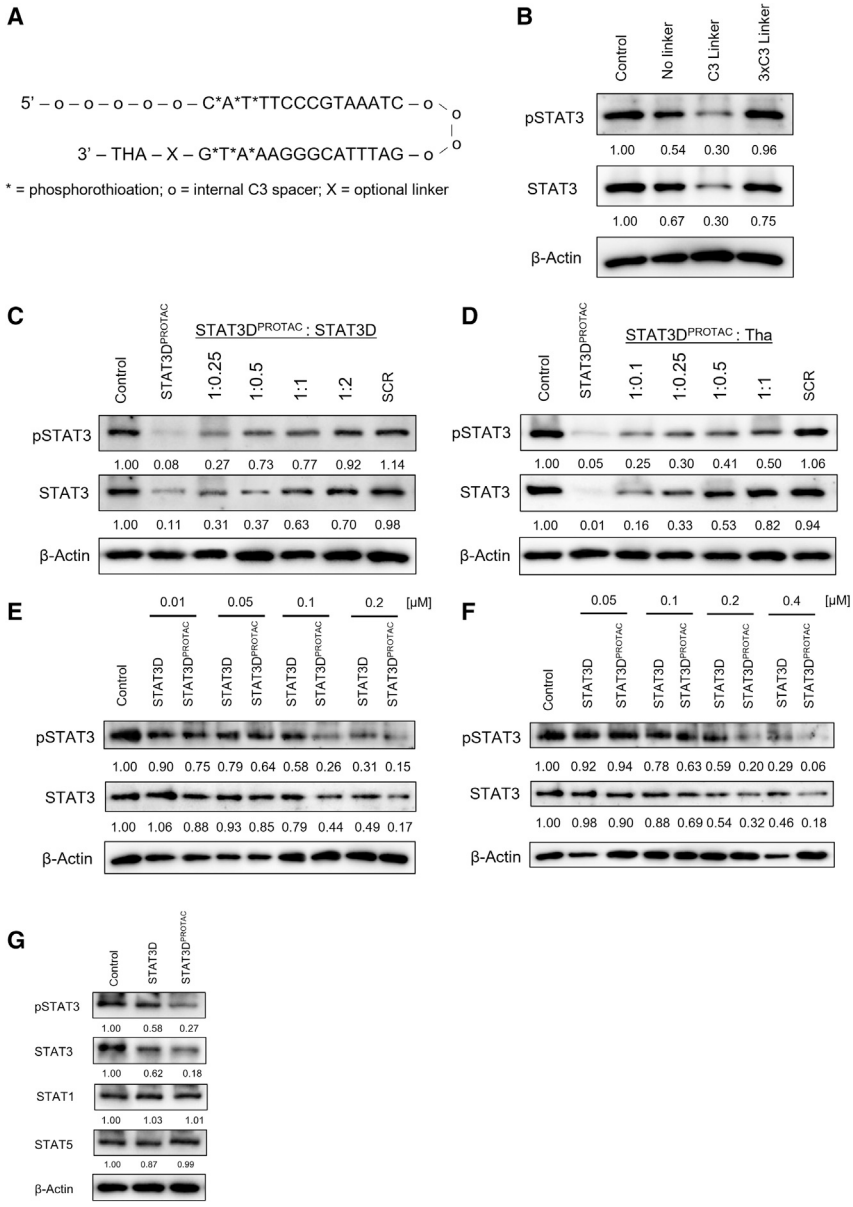

Figure 2. The optimization of STAT3dODN^{PROTAC} design to target STAT3 in mouse target cells

(A) The sequence of thalidomide-conjugated STAT3 decoy conjugate (STAT3DPROTAC). (B) Selection of the optimal linker length for tethering thalidomide to STAT3D ODN. Mouse DC2.4-S3C cells were transfected using 100 nM of the three STAT3DPROTAC variants with different linker lengths. Cells were treated with IL-6 to activate STAT3, and then protein lysates were analyzed using western blotting with β-actin as a loading control. Levels of activated and total STAT3 were digitally quantified, normalized to β-actin, and shown as a ratio relative to the untreated sample. (C and D) The competition studies to assess contributions of decoy ODN (C) and thalidomide (D) moieties to the overall STAT3DPROTAC activity. DC2.4-S3C cells were transfected using 100 nM STAT3DPROTAC together with increasing molar ratios of unconjugated STAT3 decoy (STAT3D) or thalidomide molecules; the scrambled ODN was used as a negative control. Levels of phosphorylated and total STAT3 protein were quantified as described and normalized to the untreated sample. (E and F) STAT3DPROTAC reduces STAT3 activity and expression in target mouse myeloid DC2.4-S3C cells (E) and A20 B lymphoma cells (F). Cultured cells were transfected using various concentrations of STAT3DPROTAC or STAT3D alone. Total and phosphorylated STAT3 protein levels were normalized to the untreated sample and quantified as before. (G) STAT3DPROTAC inhibits selectively STAT3 but not closely related STAT1 or STAT5. DC2.4-S3C cells were transfected using 100 nM of STAT3DPROTAC or STAT3D before the evaluation of STAT protein levels. Shown are representative results from one of three repeated experiments.

STAT3DPROTAC, and the full E3 ligase complex suggested two potential ubiquitination sites in STAT3 at lysine residues 601 and 626, which were localized in the vicinity of E2 subunit active site (Figure 3E). Others have also suggested K601 and K626 among putative candidate ubiquitination sites within STAT3.[31] Thus, we engineered point-mutated STAT3 protein variants with one or both lysine residues mutated to alanine and expressed in DC2.4 cells with wild-type STAT3 eliminated using CRISPR. DC2.4-STAT3KO cells were lentivirally transduced with point-mutated K601A and/or K626A variants of STAT3 and after selection, transfected using STAT3DPROTAC. We also verified that both point mutations did not affect STAT3 function as assessed measuring cytokine-induced STAT3 phosphorylation (Figure S3B). As shown in Figure 3F, each of the ubiquitination sites seemed necessary for the proteolytic degradation of STAT3 as indicated by the loss of 80%–90% of STAT3DPROTAC effect in cells expressing STAT3 K601A or K626A variants (Figure 3F). The double-mutant STAT3 K601A/K626A showed a complete resistance to STAT3DPROTAC-induced degradation (Figure 3F). These results suggest that both lysine residues serve as non-redundant ubiquitination sites for STAT3DPROTAC-induced and CRBN-mediated proteolytic degradation of STAT3.

Targeted delivery of CpG-conjugated STAT3D^{PROTAC} inhibits growth of human B cell lymphoma xenotransplants in mice

After verifying the proteolytic and selective mechanism of STAT3DPROTAC action, we equipped the 5′ end of decoy molecule with an a CpG oligonucleotide (D19) as outlined earlier (Figure 1A). The specific CpG part of complete C-STAT3DPROTAC was shown to act as a targeting moiety facilitating selective uptake by TLR9-expressing immune cells, such as cells of myeloid or B cell lineage

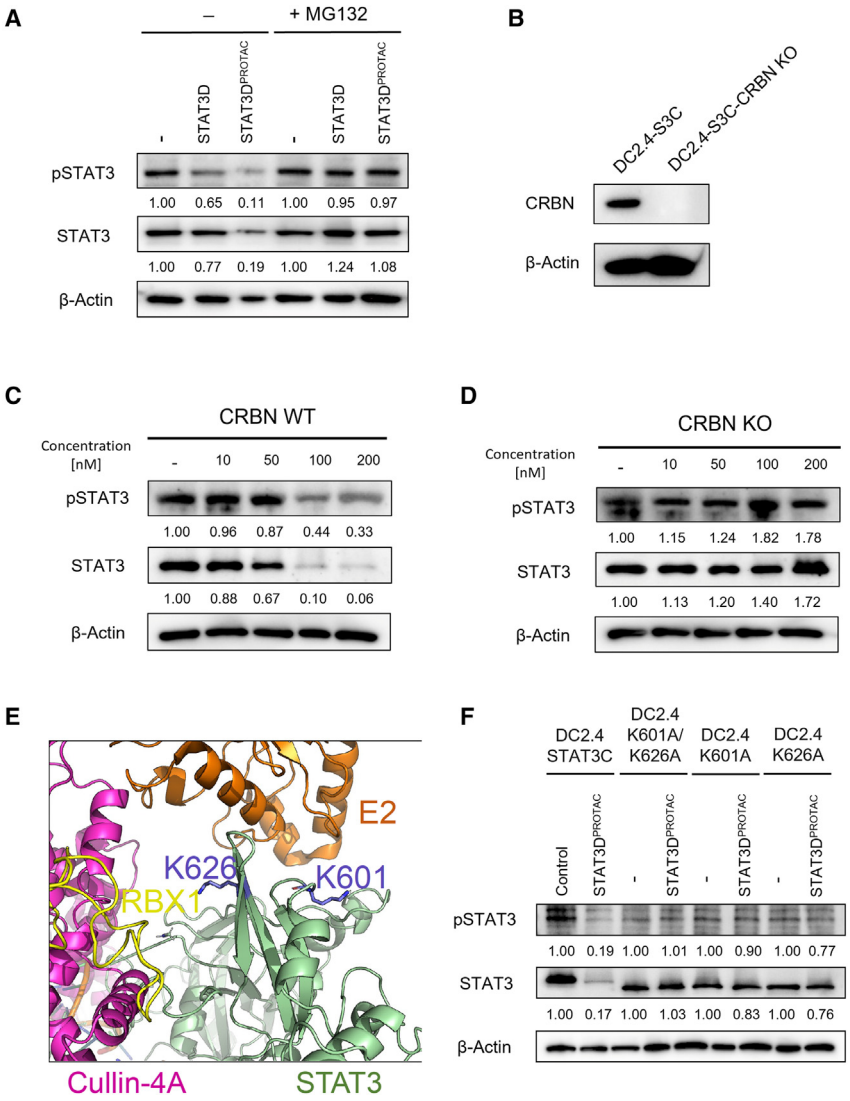

Figure 3. STAT3D^{PROTAC} induces CRBN-mediated proteasomal degradation of STAT3 targeting specific lysine residues

(A) STAT3 inhibition by STAT3DPROTAC depends on proteosome activity. DC2.4-S3C cells were pretreated using 1 μM MG-132, then transfected with 250 nM of STAT3DPROTAC or STAT3D alone and stimulated with IL-6 before harvesting. Total and phosphorylated STAT3 protein levels were normalized to the untreated sample and quantified. (B–D) STAT3 degradation by STAT3DPROTAC is CRBN-dependent. DC2.4-S3C cells expressing (B and C) or lacking CRBN (B and D) were treated transfected with increasing concentrations of STAT3DPROTAC or STAT3D and analyzed for STAT3 activation/protein levels using β-actin as an internal control. (E) Computational modeling of the interaction between STAT3DPROTAC-bound E3 ligase complex, specifically RBX1 catalytic site, and STAT3 SH2 domain indicating putative ubiquitination sites at lysine residues. (F) DC2.4 cells stably expressing point-mutated STAT3 variants with lysine to alanine mutations at K601 and/or K626 were transfected with 100 nM STAT3DPROTAC or STAT3D alone. Cell lysates were analyzed using western blotting, and β-actin was used as the internal control. Total and phosphorylated STAT3 protein levels compared with the untreated sample. Shown are representative results from one of three repeated experiments.

including tumor-associated myeloid cells or B cell lymphoma cells (Figure S4).[16,17,27] We first tested the effect of the C-STAT3DPROTAC conjugate without any transfection reagents on mouse TLR9-positive A20 B cell lymphoma cells. A20 lymphoma was extensively tested as a target for decoy-based strategies in our previous studies.[17,18,32] Within 24 h, C-STAT3DPROTAC dose-dependently reduced total STAT3 levels, with inhibition reaching maximum of 85% at 2 μM concentration (Figure 4A). In contrast, the effect of negative control treatment using an equimolar mixture of unconjugated STAT3D ODN and thalidomide was negligible (Figure 4A). As with the original STAT3DPROTAC, the CpG-conjugated molecule had specifically inhibited STAT3 but not STAT1 or STAT5 (Figures 2G, S3A, and S5A) and the presence of CpG sequence did not reduce oligo-PROTAC activity (Figure S5B). In addition, we also verified that C-STAT3DPROTAC-mediated STAT3 degradation likely requires neddylation and activation of Cullin-RING ligases (CRLs), as MLN4924 (Pevonedistat), a protein neddylation inhibitor, abrogated most of the oligo-PROTAC effect (Figure S5C). Next, we assessed the ability of C-STAT3DPROTAC to target oncogenic STAT3 signaling in human diffuse large B cell lymphoma (DLBCL) cells. As shown in Figure 4B, C-STAT3DPROTAC dose-dependently reduced activation and protein levels of STAT3 in OCI-Ly18 lymphoma cells to greater extent than the control treatment using equimolar amounts of unconjugated C-STAT3D and thalidomide, 67% vs. 24% at 1 μM dosing, respectively. The detectable inhibitory effect of the high concentrations of reference C-STAT3D plus thalidomide treatment was likely an effect of decoy molecule interfering with autoregulation of STAT3 expression in human DLBCL cells, as reported earlier.[17] Treatment with C-STAT3DPROTAC augmented downregulation of STAT3 target genes critical for lymphoma cell survival and proliferation such as *BCL2L1*, *CCND2*, *MYC*, and proinflammatory *IL12B* compared with C-STAT3D/thalidomide (Figure 4C). To verify the potential superiority of C-STAT3DPROTAC over the standard decoy design for targeting STAT3 survival signaling, we compared these two approaches in immunodeficient NSG mice bearing rapidly progressing human DLBCL. In fact, the repeated intratumoral injections of C-STAT3DPROTAC (5 mg/kg) reduced tumor volume more than twice as effectively as the standard C-STAT3D (Figure 5A). Furthermore, tumors regressed in mice treated using C-STAT3DPROTAC

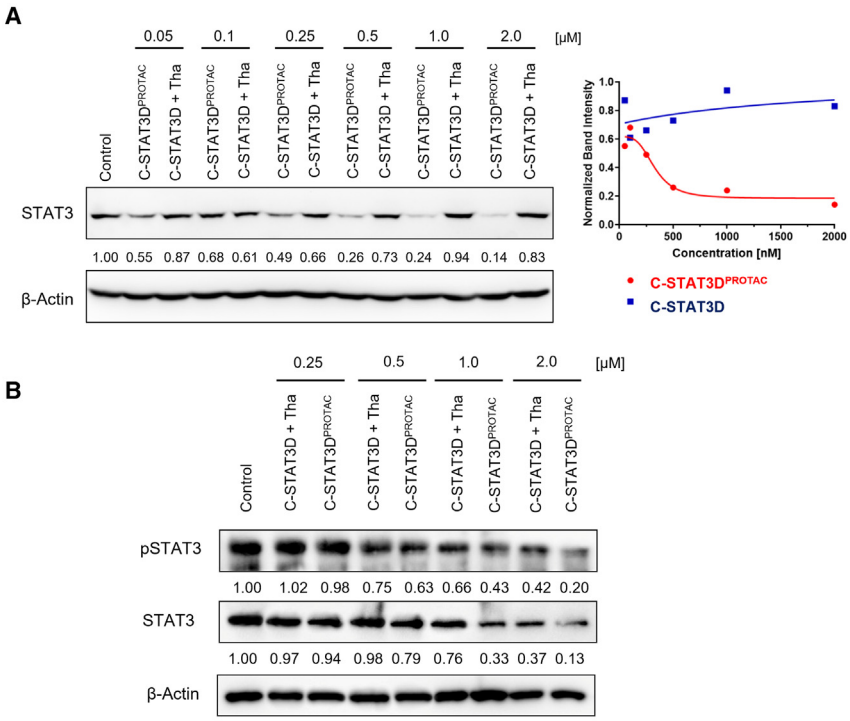

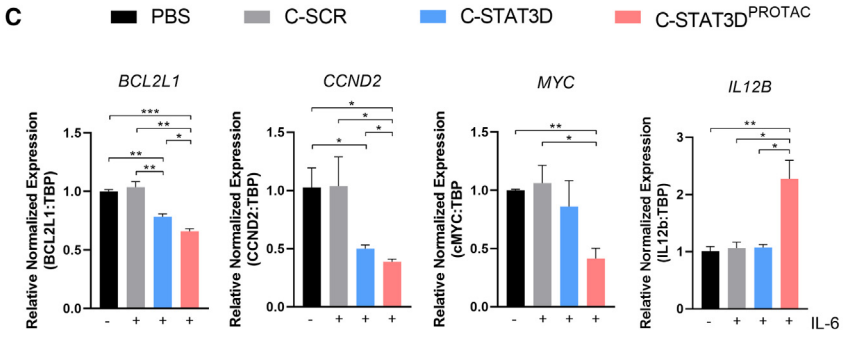

Figure 4. Targeted delivery of CpG-conjugated STAT3D^{PROTAC} inhibits growth of human B cell lymphoma *in vitro* and in immunodeficient mice

(A) Naked CpG-conjugated C-STAT3DPROTAC dose-dependently reduces STAT3 protein levels in target A20 B cell lymphoma cells. Lymphoma cells were treated using increasing concentrations of C-STAT3DPROTAC or an equimolar mixture of C-STAT3D with thalidomide. Total STAT3 protein levels were normalized to the untreated sample; left panel: representative western blot results with quantification; right panel: graph of STAT3 protein levels with non-linear fit. Shown are representative data of two independent experiments. (B) Human OCI-Ly18 B cell lymphoma cells were treated using C-STAT3DPROTAC or C-STAT3D plus thalidomide daily for 3 days. Cell lysates were analyzed using western blotting and β-actin was used as internal control. Total STAT3 protein levels were normalized to β-actin and compared with the untreated sample. (C) Human OCI-Ly3 cells were treated using C-STAT3DPROTAC, C-STAT3D plus thalidomide, or C-ScrODN over 3 days and stimulated with IL-6 before harvesting. Gene expression was examined using qRT-PCR and *TBP* as a housekeeping gene. Gene expression levels were normalized to the untreated control of OCI-Ly3 cells. Data are shown as mean ± SEM (n = 3). The p values are indicated by asterisks: *p < 0.05; **p < 0.01; ***p < 0.001.

while treatments with C-STAT3D or the negative control C-SCR only delayed lymphoma progression (Figure 5B). The protein analysis of whole tumors, indicated stronger inhibition of STAT3 activity by C-STAT3DPROTAC than C-STAT3D, although the overall levels if STAT3 were reduced in both cases (Figure 5C). Overall, our results suggest that C-STAT3DPROTAC design provides superior, direct efficacy against human DCBCL over the reversible decoy inhibitor at least in the immunodeficient mice.

DISCUSSION

By combining rational design with structure-based computational analysis, we demonstrated that incorporating PROTAC activity into a cell-selective STAT3 decoy-based inhibitor can dramatically improve target inhibition and thereby the direct *in vivo* antitumor efficacy. We have previously shown that CpG-conjugated STAT3 decoy strategy results in potent immune-mediated antitumor responses against models of AML and B cell lymphoma in immunocompetent mice.[16,17] However, the reversibility of STAT3 inhibition by these strategies limited the direct cytotoxicity to leukemia and lymphoma cells which is an important therapeutic effect in patients' with advanced and rapidly progressing tumors. Our results underscore the potential of using the existing decoy ODN-based oligonucleotides for the design of proteolytic degraders of undruggable TFs, such as STAT3.[2,5] The oligo-PROTAC design offers high molecular target specificity on the basis of the TF-specific DNA sequence recognition, which is not affected by 3′-end modifications. As shown by the results of molecular modeling, the simplicity of oligo-PROTAC design allows fine-tuning of the interaction between the protein target and the E3 ubiquitin ligase complex to maximize POI degradation. Furthermore, the support of modeling tools facilitates mode-of-action studies and permits the identification of targeted lysine residues in the POI. Our original strategy of *in silico* modeling and MD-driven optimization of the oligo-PROTAC has successfully overcome challenges in the modeling of a massive protein-oligonucleotide complex. These included lack of structural information on how E3 ligase interacts with STAT3 in presence of an oligo-PROTAC on the basis of STAT3 decoy ODN. All reported PROTAC crystal structures involved not oligonucleotides but small molecules complexed between CRBN and target proteins. We believe that this is the first model and all-atom MD simulation of all components of E3 ligase such as CRBN, DDB1, Cullin4A, RBX1, and E2 bound to

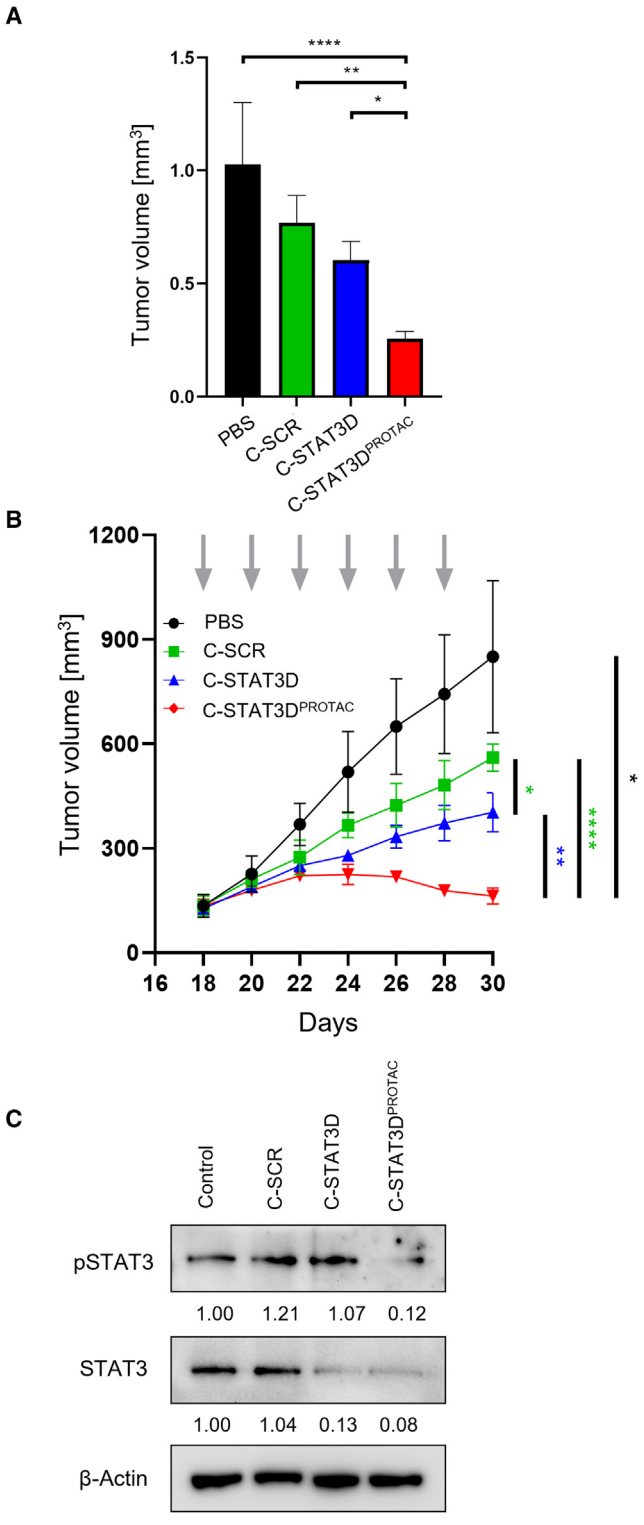

Figure 5. Targeted delivery of CpG-conjugated STAT3D^{PROTAC} inhibits growth of human B cell lymphoma in immunodeficient mice

(A–C) Intratumoral administration of C-STAT3DPROTAC inhibits growth of OCI-Ly3 B cell lymphoma xenotransplants in immunodeficient NSG mice. Ten million OCI-Ly3 cells were engrafted subcutaneously, and mice with established lymphomas (~100 mm^3) were injected 6 times every other day using 5 mg/kg C-STAT3DPROTAC, C-STAT3D, C-SCR ODN, or PBS. Tumors were harvested two days after the final injection to assess tumor volume (B), compared with tumor growth kinetics (C) and levels of STAT3 proteins in the whole tumors; data are shown as mean ± SEM (n = 4). The p values are indicated by asterisks: *p < 0.05; **p < 0.01; ****p < 0.0001.

oligo-PROTAC-associated TF, with an experimental confirmation of ubiquitination site predictions.

Although PROTAC technology first appeared in the early 2000s, the unique potential of targeting previously undruggable proteins through lower affinity binding has brought a burgeoning number of studies and led to recent clinical trials.[33] Our findings represent the first demonstration of feasibility to inhibit STAT3 signaling using oligo-PROTAC design *in vitro* and *in vivo*. Although STAT3-specific PROTACs have recently been described,[26,34] these small molecule conjugates do not offer cell selectivity, which is a crucial consideration because of the role of STAT3 in non-malignant cells, including T cells.[6,14]

Others have recently shown the potential to target oncogenic TFs, such as LEF1 and ERG, using specific double-stranded ODNs, resulting in proteolytic degradation of target proteins and reduced prostate cancer cell survival and proliferation.[35,36] Beyond TFs, it seems feasible to use short RNA oligonucleotides for generating PROTAC molecules targeting RNA-binding oncoproteins.[37] Despite these rapid advances, lack of targeted delivery methods hampers further translation of these approaches to clinical application.[15,38] Although significant progress in LNP formulations of RNA enabled rapid advancement in locally administered mRNA vaccines against viral diseases and cancer, the systemic administration of oligonucleotides to organs other than liver or to specific cellular targets remains a challenge.[39] Our study provides evidence that it is feasible to equip oligo-PROTACs with specific targeting domains without interfering with the POI/E3 ligase complex and thereby facilitating cell-selective delivery of the naked and unformulated ODN conjugates. C-STAT3DPROTAC and the original C-STAT3D use CpG ODN to target scavenger receptors on the variety of immune cells. These include B lymphocytes and myeloid cells, such as DCs and macrophages, as well as cancer cells, e.g., AML, B cell lymphoma cells, or certain solid tumor cells in prostate cancers and glioma.[15–17] Importantly, the interaction with endosomal TLR9 facilitates the rapid release of CpG conjugates into the cytosol and augments potency of these oligonucleotides.[16,40]

Overall, our proof-of-concept studies on the cell-selective C-STAT3DPROTAC design highlight the potential of using oligo-PROTAC design for cancer therapy. Further optimization of C-STAT3DPROTAC will focus on the key issues of molecule stability/bioavailability, immunostimulatory activity, and tolerability. Given that siRNA- or ASO-based CpG-STAT3 inhibitors as well as various small-molecule PROTACs have reached or are near clinical

testing, we believe that C-STAT3DPROTAC has potential to provide safe and effective treatment for patients with B cell lymphoma and potentially other cancer indications.

MATERIALS AND METHODS

Cells

Human OCI-Ly3 B cell lymphoma line was purchased from Deutsche Sammlung von Mikroorganismen und Zellkulturen (DSMZ). Human OCI-Ly18 cells were provided by Dr. Larry Kwak (City of Hope [COH], Duarte, CA). Mouse dendritic DC2.4 cells were originally from Dr. Kenneth Rock (University of Massachusetts Medical School). The mouse A20 B cell lymphoma line was purchased from American Type Culture Collection (ATCC; Manassas, VA). DC2.4, A20, OCI-Ly3, and OCI-Ly18 cells were cultured in RPMI1640 with 10%–20% fetal bovine serum (FBS). To generate DC2.4 cells with constitutively activated STAT3C (DC2.4-S3C)[30] or point-mutated K601A and K626A STAT3 variants, expression plasmids were designed and purchased from VectorBuilder (Chicago, IL), then cloned into a third-generation lentiviral vector (pMDLg/pRRE/pRSV-Rev/pMD2.G). The STAT3 mutation-bearing lentiviral vectors were then transduced into DC2.4-CRISPR-STAT3KO cells, mutant cells were selected for with puromycin, and GFP$^+$ cells were sorted. All cells were regularly tested for mycoplasma contamination using the LookOut mycoplasma PCR detection kit (Sigma-Aldrich, St. Louis, MO).

Mice

All animal experiments were carried out in accordance with established institutional guidance and approved protocols from the institutional animal care and use committee (COH). *NOD/SCID/IL-2Rγ KO* (NSG) mice, originally obtained from the Jackson Laboratory (Bar Harbor, ME), were maintained at COH. Mice were injected subcutaneously with 10^7 OCI-Ly3 cells in PBS and lymphoma engraftment and progression were monitored by caliper measurements.

Oligonucleotide design

All of the following oligonucleotides were synthesized in the DNA/RNA Synthesis Core (COH) as previously described[27] and then conjugated to modified thalidomide moiety using click chemistry as shown in the Figure S1. The resulting conjugates are illustrated below (where o = internal C3 spacer, X = 3′-C6-amino linker, * = phosphorothioation, and THA = thalidomide).

C-STAT3dODN

5′-G*G*TGCATCGATGCAGG*G*G*G*G – o – o – o – o – o – C*A*T*TTCCCGTAAATC – o – o – o – o – GATTTACGGGAA*A*T*G-3′

C-scrODN

5′-G*G*TGCATCGATGCAGG*G*G*G*G – o – o – o – o – o – A*C*T*CTTGCCAATTAC – o – o – o – o – GTAATTGGCAAG*A*G*T-3′

C-STAT3dODN^{PROTAC} (no linker)

5′-G*G*TGCATCGATGCAGG*G*G*G*G – C*A*T*TTCCCGTAAATC – o – o – o – o – GATTTACGGGAA*A*T*G – THA-3′

C-STAT3dODN^{PROTAC} (single linker unit)

5′-G*G*TGCATCGATGCAGG*G*G*G*G – o – o – o – o – o – C*A*T*TTCCCGTAAATC – o – o – o – o – GATTTACGGGAA*A*T*G – o – THA-3′

C-STAT3dODN^{PROTAC} (three linker units)

5′-G*G*TGCATCGATGCAGG*G*G*G*G – o – o – o – o – o – C*A*T*TTCCCGTAAATC – o – o – o – o – GATTTACGGGAA*A*T*G – o – o – o – THA-3′

Computational methods

Modeling of initial STAT3/CRBN/PROTAC ternary complex structure

The crystal structure of a decoy oligonucleotide-bound STAT3 dimer was downloaded from the Protein Data Bank (PDB: 1BG1).[41] The structure was prepared using Protein Preparation Wizard[42] in Maestro, by adding hydrogen atoms and the missing residues, followed by minimization using MacroModel.[43] The CpG and linker moieties were attached to the decoy oligonucleotide using molecular modeling in Maestro. Lenalidomide-bound CRBN structure was downloaded from the PDB (PDB: 5FQD)[44] and placed close to the PROTAC linker of STAT3 using rigid body transformations in Maestro. Thalidomide was modeled by modifying the bound lenalidomide in CRBN, followed by the addition of covalent bond with the C6-amino linker (Figure S2A). The entire complex was then minimized using PrimeX.[45]

Initial structure preparation

The initial CRBN/PROTAC bound STAT3 structure was parameterized in AMBER16[46,47] using the FF14SBonlySC[48] and Parmbsc1[49] force fields for protein and nucleic acid segments respectively. The linkers and thalidomide moieties were parameterized using the GAFF2 force field.[50] Partial charges were obtained by fitting a restrained coulomb function to the electrostatic potential (RESP)[51] obtained using JAGUAR.[52] The partial charges were calculated using the online R.E.D. server.[53]

System setup for implicit solvent MD

MD simulations were performed in the NVT ensemble using the IGB8 generalized Born implicit solvation model (igb = 8)[54] and AMBER16 MD simulation program. A temperature of 290 K was controlled using the Langevin thermostat with $\gamma = 1$.[55] No periodic boundary conditions were used as implemented in the implicit solvent simulations in AMBER. The rgbmax cutoff, that determines the maximum distance between atoms pairs used in calculating the effective Born radii, was set to 15 Å. The non-bond interactions were calculated explicitly for all atom pairs without any distance cutoff. An effective salt concentration of 0.15 M was set as part of the generalized Born parameters (saltcon = 0.15). Finally, hydrogen mass repartitioning was applied in order to use a timestep of 4 fs.[56] The MD snapshots were saved every 40 ps.

System equilibration

The system was initially subjected to 20,000 steps of minimization, of which the first 2,500 steps were using the steepest descent method, followed by conjugate gradient for the rest. Next, the system was heated from 0 to 290 K over a period of 10 ns. During this step, harmonic restraints were applied to all heavy atoms with a force constant of 5 kcal/mol. Then the system was equilibrated at a constant temperature of 290 K for 10 ns, when the harmonic restraints were gradually decreased to zero.

Simulating the binding of PROTAC-bound CRBN to STAT3

Commencing from the final frame of the equilibration step, a 100 ns of unrestrained MD simulation was performed. Throughout the initial half of the simulation, the PROTAC tethered CRBN diffused toward STAT3, leading to their binding, and remained bound for the rest of the simulation. The last frame from the unrestrained MD trajectory was used as the model for STAT3/CRBN/PROTAC complex presented in this report. We performed three replicates of MD simulations, with each replicate starting from the heating step, followed by equilibration and unrestrained MD, resulting in bound complexes.

Binding free energy calculation

From the three replicate MD simulations, the last 50 ns (as the first 50 ns represented the diffusion of CRBN toward STAT3) was used for calculating binding free energies of STAT3 with CRBN in presence and absence of oligo-PROTAC. Binding free energy calculations were performed using the MMPBSA method[57] available as part of the AMBER software package.

Center-of-mass distance calculations between STAT3 and CRBN

For each MD frame, the center-of-mass coordinates of CRBN and STAT3 were calculated using the heavy atoms in each protein. These center-of-mass coordinates were then used to calculate the distance between CRBN and STAT3 as function of time, as shown in Figure S2B.

Selection of STAT3/CRBN/PROTAC complex structure

We selected the last frame from the final 100 ns trajectory from each replicate MD and constructed the full E3 ligase complex, as described below. Out of the three models thus generated, the structural model that showed the least number of clashes between ligase and STAT3 (discerned through manual visualization in PyMOL) was selected as the final model discussed in this paper.

Modeling of the STAT3/PROTAC bound E3 ubiquitin ligase

The crystal structure of CRBN bound to DDB1, Cullin4A, and RBX1 was downloaded from PDB (PDB: 2HYE).[58] This structure was then aligned to the CRBN-bound STAT3 complex using PyMOL.[59] Next, the crystal structure of RNF4 (RING domain protein playing a similar role as RBX1 in recruiting E2) bound to E2 was downloaded from PDB (PDB: 4AP4) and aligned to the RBX1 moiety from the CRBN-DDB1-Cullin4A-RBX1 structure.[60] Finally, the DDB1, Cullin4A, and E2 moieties from the two crystal structures were combined with the CRBN-bound STAT3 to obtain the entire E3 ligase complex. In the final model, a local clash between the CpG moiety of the PROTAC and the E3 ligase was resolved using the sculpting feature of Maestro, followed by minimization of the first 8 nt of the CpG using Prime,[45] while keeping the rest of the structure rigid. This final structure was used to generate Figures 1C, S2D, and S2E.

Transcriptomic and protein assays

For qPCR, total RNA was extracted from cultured cells using the Maxwell RSC simplyRNA Cells system (AS1390; Promega, Madison, WI), then reverse transcribed into cDNAs with the iScript cDNA synthesis kit (Bio-Rad). The qPCR was then carried out using specific primers for *BCL2L1*, *CCND2*, *MYC*, *IL12B*, and *TBP* as previously described[61,62] with a CFX96 Real-Time PCR Detection System (Bio-Rad). Western blots were performed and described previously[61] using antibodies specific to pSTAT3, STAT3, STAT1, STAT5 (Cell Signaling Technology, Danvers, MA), or β-actin-HRP (horseradish peroxidase) (Sigma-Aldrich). Blots were imaged in a Bio-Rad Chem-iDoc MP System using enhanced chemiluminescence (ECL; SuperSignal West Femto Maximum Sensitivity Substrate), and the resulting images were analyzed using accompanying Bio-Rad Image Lab software and Prism 8 (GraphPad). Cytokine levels in cell culture supernatants were measured using the Luminex system.

Statistical analysis

An unpaired t test was used to determine the statistical significance of differences between two treatment groups. Two-way ANOVA and Bonferroni post-tests were used to estimate the statistical significance of differences between multiple treatment groups. The relationship between two groups was determined using correlation and linear regression. The p values are indicated in figures with asterisks (*$p < 0.05$, **$p < 0.01$, ***$p < 0.001$, and ****$p < 0.0001$). Data were analyzed using Prism version 8.4.3 software.

DATA AND CODE AVAILABILITY

All data and reagents generated within this study are available from the corresponding author upon a reasonable request.

SUPPLEMENTAL INFORMATION

Supplemental information can be found online at https://doi.org/10.1016/j.omtn.2024.102137.

ACKNOWLEDGMENTS

We are grateful to the staff at Analytical Cytometry, DNA/RNA Synthesis, Analytical Pharmacology, and Animal Resource Cores (COH). We appreciate support from Dr. D. Kaniowski in the preparation of this manuscript. This work was supported in part by National Cancer Institute/National Institutes of Health awards R01CA284593 (M.K.), P50CA107399 (S.F.), and P30CA033572 (COH). The content is solely the responsibility of the authors and does not necessarily represent the official views of the National Institutes of Health.

AUTHOR CONTRIBUTIONS

Conceptualization, M.K., P.S., and N.V.; methodology, Z.Z., J.H., S.B., and D.W.; investigation, J.H., Z.Z., Y.L., and D.W.; writing – original draft, Z.Z., J.H., and M.K.; writing – review & editing, M.K.; funding acquisition, M.K., L.K., and S.F.; resources, P.S. and M.K.; supervision, M.K.

DECLARATION OF INTERESTS

M.K. and P.S. are named on the patent application submitted by COH that covers the design of oligonucleotides presented in this report. M.K. is a scientific advisor to Scopus Biopharma and Duet Biotherapeutics, two companies developing oligonucleotide therapeutics.

REFERENCES

1. Yu, H., Kortylewski, M., and Pardoll, D. (2007). Crosstalk between cancer and immune cells: role of STAT3 in the tumour microenvironment. Nat. Rev. Immunol. *7*, 41–51. https://doi.org/10.1038/nri1995.
2. Li, Y.-J., Zhang, C., Martincuks, A., Herrmann, A., and Yu, H. (2023). STAT proteins in cancer: orchestration of metabolism. Nat. Rev. Cancer *23*, 115–134. https://doi.org/10.1038/s41568-022-00537-3.
3. Erdogan, F., Radu, T.B., Orlova, A., Qadree, A.K., de Araujo, E.D., Israelian, J., Valent, P., Mustjoki, S.M., Herling, M., Moriggl, R., and Gunning, P.T. (2022). JAK-STAT core cancer pathway: An integrative cancer interactome analysis. J. Cell. Mol. Med. *26*, 2049–2062. https://doi.org/10.1111/jcmm.17228.
4. Philips, R.L., Wang, Y., Cheon, H., Kanno, Y., Gadina, M., Sartorelli, V., Horvath, C.M., Darnell, J.E., Jr., Stark, G.R., and O'Shea, J.J. (2022). The JAK-STAT pathway at 30: Much learned, much more to do. Cell *185*, 3857–3876. https://doi.org/10.1016/j.cell.2022.09.023.
5. Johnson, D.E., O'Keefe, R.A., and Grandis, J.R. (2018). Targeting the IL-6/JAK/STAT3 signalling axis in cancer. Nat. Rev. Clin. Oncol. *15*, 234–248. https://doi.org/10.1038/nrclinonc.2018.8.
6. Su, Y.-L., Banerjee, S., White, S.V., and Kortylewski, M. (2018). STAT3 in Tumor-Associated Myeloid Cells: Multitasking to Disrupt Immunity. Int. J. Mol. Sci. *19*, 1803. https://doi.org/10.3390/ijms19061803.
7. Yeh, J.E., Toniolo, P.A., and Frank, D.A. (2013). Targeting transcription factors: promising new strategies for cancer therapy. Curr. Opin. Oncol. *25*, 652–658. https://doi.org/10.1097/01.cco.0000432528.88101.1a.
8. Brachet-Botineau, M., Polomski, M., Neubauer, H.A., Juen, L., Hédou, D., Viaud-Massuard, M.C., Prié, G., and Gouilleux, F. (2020). Pharmacological inhibition of oncogenic STAT3 and STAT5 signaling in hematopoietic cancers. Cancers *12*, 240. https://doi.org/10.3390/cancers12010240.
9. Sen, M., Thomas, S.M., Kim, S., Yeh, J.I., Ferris, R.L., Johnson, J.T., Duvvuri, U., Lee, J., Sahu, N., Joyce, S., et al. (2012). First-in-human trial of a STAT3 decoy oligonucleotide in head and neck tumors: implications for cancer therapy. Cancer Discov. *2*, 694–705. https://doi.org/10.1158/2159-8290.CD-12-0191.
10. Hong, D., Kurzrock, R., Kim, Y., Woessner, R., Younes, A., Nemunaitis, J., Fowler, N., Zhou, T., Schmidt, J., Jo, M., et al. (2015). AZD9150, a next-generation antisense oligonucleotide inhibitor of STAT3 with early evidence of clinical activity in lymphoma and lung cancer. Sci. Transl. Med. *7*, 314ra185. https://doi.org/10.1126/scitranslmed.aac5272.
11. Reilley, M.J., McCoon, P., Cook, C., Lyne, P., Kurzrock, R., Kim, Y., Woessner, R., Younes, A., Nemunaitis, J., Fowler, N., et al. (2018). STAT3 antisense oligonucleotide AZD9150 in a subset of patients with heavily pretreated lymphoma: results of a phase 1b trial. J. Immunother. Cancer *6*, 119. https://doi.org/10.1186/s40425-018-0436-5.
12. Corey, D.R., Damha, M.J., and Manoharan, M. (2022). Challenges and opportunities for nucleic acid therapeutics. Nucleic Acid Ther. *32*, 8–13. https://doi.org/10.1089/nat.2021.0085.
13. Fraietta, J.A., Lacey, S.F., Orlando, E.J., Pruteanu-Malinici, I., Gohil, M., Lundh, S., Boesteanu, A.C., Wang, Y., O'Connor, R.S., Hwang, W.T., et al. (2018). Determinants of response and resistance to CD19 chimeric antigen receptor (CAR) T cell therapy of chronic lymphocytic leukemia. Nat. Med. *24*, 563–571. https://doi.org/10.1038/s41591-018-0010-1.
14. Kaminskiy, Y., and Melenhorst, J.J. (2022). STAT3 Role in T-Cell Memory Formation. Int. J. Mol. Sci. *23*, 2878. https://doi.org/10.3390/ijms23052878.
15. Kortylewski, M., and Moreira, D. (2017). Myeloid cells as a target for oligonucleotide therapeutics: turning obstacles into opportunities. Cancer Immunol. Immunother. *66*, 979–988. https://doi.org/10.1007/s00262-017-1966-2.
16. Zhang, Q., Hossain, D.M.S., Duttagupta, P., Moreira, D., Zhao, X., Won, H., Buettner, R., Nechaev, S., Majka, M., Zhang, B., et al. (2016). Serum-resistant CpG-STAT3 decoy for targeting survival and immune checkpoint signaling in acute myeloid leukemia. Blood *127*, 1687–1700. https://doi.org/10.1182/blood-2015-08-665604.
17. Zhao, X., Zhang, Z., Moreira, D., Su, Y.L., Won, H., Adamus, T., Dong, Z., Liang, Y., Yin, H.H., Swiderski, P., et al. (2018). B Cell Lymphoma Immunotherapy Using TLR9-Targeted Oligonucleotide STAT3 Inhibitors. Mol. Ther. *26*, 695–707. https://doi.org/10.1016/j.ymthe.2018.01.007.
18. Zhang, Z., Zhao, X., Wang, D., Moreira, D., Su, Y.L., Alcantara, M., Swiderski, P., Wong, J., Hui, S., Forman, S., et al. (2021). Targeted In Vivo Delivery of NF-κB Decoy Inhibitor Augments Sensitivity of B Cell Lymphoma to Therapy. Mol. Ther. *29*, 1214–1225. https://doi.org/10.1016/j.ymthe.2020.11.026.
19. Békés, M., Langley, D.R., and Crews, C.M. (2022). PROTAC targeted protein degraders: the past is prologue. Nat. Rev. Drug Discov. *21*, 181–200. https://doi.org/10.1038/s41573-021-00371-6.
20. Bushweller, J.H. (2019). Targeting transcription factors in cancer - from undruggable to reality. Nat. Rev. Cancer *19*, 611–624. https://doi.org/10.1038/s41568-019-0196-7.
21. Paiva, S.-L., and Crews, C.M. (2019). Targeted protein degradation: elements of PROTAC design. Curr. Opin. Chem. Biol. *50*, 111–119. https://doi.org/10.1016/j.cbpa.2019.02.022.
22. Smith, B.E., Wang, S.L., Jaime-Figueroa, S., Harbin, A., Wang, J., Hamman, B.D., and Crews, C.M. (2019). Differential PROTAC substrate specificity dictated by orientation of recruited E3 ligase. Nat. Commun. *10*, 131. https://doi.org/10.1038/s41467-018-08027-7.
23. Bondeson, D.P., Mares, A., Smith, I.E.D., Ko, E., Campos, S., Miah, A.H., Mulholland, K.E., Routly, N., Buckley, D.L., Gustafson, J.L., et al. (2015). Catalytic in vivo protein knockdown by small-molecule PROTACs. Nat. Chem. Biol. *11*, 611–617. https://doi.org/10.1038/nchembio.1858.
24. Winter, G.E., Buckley, D.L., Paulk, J., Roberts, J.M., Souza, A., Dhe-Paganon, S., and Bradner, J.E. (2015). Phthalimide conjugation as a strategy for in vivo target protein degradation. Science *348*, 1376–1381. https://doi.org/10.1126/science.aab1433.
25. Zhou, H., Bai, L., Xu, R., Zhao, Y., Chen, J., McEachern, D., Chinnaswamy, K., Wen, B., Dai, L., Kumar, P., et al. (2019). Structure-Based Discovery of SD-36 as a Potent, Selective, and Efficacious PROTAC Degrader of STAT3 Protein. J. Med. Chem. *62*, 11280–11300. https://doi.org/10.1021/acs.jmedchem.9b01530.
26. Bai, L., Zhou, H., Xu, R., Zhao, Y., Chinnaswamy, K., McEachern, D., Chen, J., Yang, C.Y., Liu, Z., Wang, M., et al. (2019). A Potent and Selective Small-Molecule Degrader of STAT3 Achieves Complete Tumor Regression In Vivo. Cancer Cell *36*, 498–511.e17. https://doi.org/10.1016/j.ccell.2019.10.002.
27. Kortylewski, M., Swiderski, P., Herrmann, A., Wang, L., Kowolik, C., Kujawski, M., Lee, H., Scuto, A., Liu, Y., Yang, C., et al. (2009). In vivo delivery of siRNA to immune cells by conjugation to a TLR9 agonist enhances antitumor immune responses. Nat. Biotechnol. *27*, 925–932. https://doi.org/10.1038/nbt.1564.
28. Mori, T., Ito, T., Liu, S., Ando, H., Sakamoto, S., Yamaguchi, Y., Tokunaga, E., Shibata, N., Handa, H., and Hakoshima, T. (2018). Structural basis of thalidomide enantiomer binding to cereblon. Sci. Rep. *8*, 1294. https://doi.org/10.1038/s41598-018-19202-7.
29. Fischer, E.S., Böhm, K., Lydeard, J.R., Yang, H., Stadler, M.B., Cavadini, S., Nagel, J., Serluca, F., Acker, V., Lingaraju, G.M., et al. (2014). Structure of the DDB1-CRBN E3 ubiquitin ligase in complex with thalidomide. Nature *512*, 49–53. https://doi.org/10.1038/nature13527.
30. Bromberg, J.F., Wrzeszczynska, M.H., Devgan, G., Zhao, Y., Pestell, R.G., Albanese, C., and Darnell, J.E., Jr. (1999). Stat3 as an oncogene. Cell *98*, 295–303. https://doi.org/10.1016/s0092-8674(00)81959-5.

31. Akimov, V., Barrio-Hernandez, I., Hansen, S.V.F., Hallenborg, P., Pedersen, A.K., Bekker-Jensen, D.B., Puglia, M., Christensen, S.D.K., Vanselow, J.T., Nielsen, M.M., et al. (2018). UbiSite approach for comprehensive mapping of lysine and N-terminal ubiquitination sites. Nat. Struct. Mol. Biol. *25*, 631–640. https://doi.org/10.1038/s41594-018-0084-y.

32. Garrido, G., Schrand, B., Levay, A., Rabasa, A., Ferrantella, A., Da Silva, D.M., D'Eramo, F., Marijt, K.A., Zhang, Z., Kwon, D., et al. (2020). Vaccination against Nonmutated Neoantigens Induced in Recurrent and Future Tumors. Cancer Immunol. Res. *8*, 856–868. https://doi.org/10.1158/2326-6066.CIR-20-0020.

33. Garber, K. (2022). The PROTAC gold rush. Nat. Biotechnol. *40*, 12–16. https://doi.org/10.1038/s41587-021-01173-2.

34. Heppler, L.N., and Frank, D.A. (2019). Inhibit versus Destroy: Are PROTAC Degraders the Solution to Targeting STAT3? Cancer Cell *36*, 459–461. https://doi.org/10.1016/j.ccell.2019.10.010.

35. Shao, J., Yan, Y., Ding, D., Wang, D., He, Y., Pan, Y., Yan, W., Kharbanda, A., Li, H.Y., and Huang, H. (2021). Destruction of DNA-Binding Proteins by Programmable Oligonucleotide PROTAC (O'PROTAC): Effective Targeting of LEF1 and ERG. Adv. Sci. *8*, e2102555. https://doi.org/10.1002/advs.202102555.

36. Yan, Y., Shao, J., Ding, D., Pan, Y., Tran, P., Yan, W., Wang, Z., Li, H.Y., and Huang, H. (2022). 3-Aminophthalic acid, a new cereblon ligand for targeted protein degradation by O'PROTAC. Chem. Commun. *58*, 2383–2386. https://doi.org/10.1039/d1cc06525d.

37. Ghidini, A., Cléry, A., Halloy, F., Allain, F.H.T., and Hall, J. (2021). RNA-PROTACs: Degraders of RNA-Binding Proteins. Angew Chem Int Ed *60*, 3163–3169. https://doi.org/10.1002/anie.202012330.

38. Roberts, T.C., Langer, R., and Wood, M.J.A. (2020). Advances in oligonucleotide drug delivery. Nat. Rev. Drug Discov. *19*, 673–694. https://doi.org/10.1038/s41573-020-0075-7.

39. Bost, J.P., Barriga, H., Holme, M.N., Gallud, A., Maugeri, M., Gupta, D., Lehto, T., Valadi, H., Esbjörner, E.K., Stevens, M.M., and El-Andaloussi, S. (2021). Delivery of oligonucleotide therapeutics: chemical modifications, lipid nanoparticles, and extracellular vesicles. ACS Nano *15*, 13993–14021. https://doi.org/10.1021/acsnano.1c05099.

40. Nechaev, S., Gao, C., Moreira, D., Swiderski, P., Jozwiak, A., Kowolik, C.M., Zhou, J., Armstrong, B., Raubitschek, A., Rossi, J.J., and Kortylewski, M. (2013). Intracellular processing of immunostimulatory CpG-siRNA: Toll-like receptor 9 facilitates siRNA dicing and endosomal escape. J. Control. Release *170*, 307–315. https://doi.org/10.1016/j.jconrel.2013.06.007.

41. Becker, S., Groner, B., and Müller, C.W. (1998). Three-dimensional structure of the Stat3beta homodimer bound to DNA. Nature *394*, 145–151. https://doi.org/10.1038/28101.

42. Sastry, G.M., Adzhigirey, M., Day, T., Annabhimoju, R., and Sherman, W. (2013). Protein and ligand preparation: parameters, protocols, and influence on virtual screening enrichments. J. Comput. Aided. Mol. Des. *27*, 221–234. https://doi.org/10.1007/s10822-013-9644-8.

43. (2013). Schrödinger Release 2013 (MacroModel, Schrödinger, LLC).

44. Petzold, G., Fischer, E.S., and Thomä, N.H. (2016). Structural basis of lenalidomide-induced CK1α degradation by the CRL4(CRBN) ubiquitin ligase. Nature *532*, 127–130. https://doi.org/10.1038/nature16979.

45. Bell, J.A., Cao, Y., Gunn, J.R., Day, T., Gallicchio, E., Zhou, Z., Levy, R., and Farid, R. (2012). *PrimeX* and the Schrödinger computational chemistry suite of programs. In International Tables for Crystallography: Crystallography of Biological Macromolecules. Vol F. International Tables for Crystallography: International Tables Online, E. Arnold, D.M. Himmel, and M.G. Rossmann, eds. (International Union of Crystallography), pp. 534–538. https://doi.org/10.1107/97809553602060000864.

46. Case, D.A., Cheatham, T.E., Darden, T., Gohlke, H., Luo, R., Merz, K.M., Jr., Onufriev, A., Simmerling, C., Wang, B., and Woods, R.J. (2005). The Amber biomolecular simulation programs. J. Comput. Chem. *26*, 1668–1688. https://doi.org/10.1002/jcc.20290.

47. Salomon-Ferrer, R., Case, D.A., and Walker, R.C. (2013). An overview of the Amber biomolecular simulation package. WIREs Comput. Mol. Sci. *3*, 198–210. https://doi.org/10.1002/wcms.1121.

48. Nguyen, H., Maier, J., Huang, H., Perrone, V., and Simmerling, C. (2014). Folding simulations for proteins with diverse topologies are accessible in days with a physics-based force field and implicit solvent. J. Am. Chem. Soc. *136*, 13959–13962. https://doi.org/10.1021/ja5032776.

49. Ivani, I., Dans, P.D., Noy, A., Pérez, A., Faustino, I., Hospital, A., Walther, J., Andrio, P., Goñi, R., Balaceanu, A., et al. (2016). Parmbsc1: a refined force field for DNA simulations. Nat. Methods *13*, 55–58. https://doi.org/10.1038/nmeth.3658.

50. He, X., Man, V.H., Yang, W., Lee, T.-S., and Wang, J. (2020). A fast and high-quality charge model for the next generation general AMBER force field. J. Chem. Phys. *153*, 114502. https://doi.org/10.1063/5.0019056.

51. Woods, R.J., and Chappelle, R. (2000). Restrained electrostatic potential atomic partial charges for condensed-phase simulations of carbohydrates. Theochem *527*, 149–156. https://doi.org/10.1016/S0166-1280(00)00487-5.

52. Bochevarov, A.D., Harder, E., Hughes, T.F., Greenwood, J.R., Braden, D.A., Philipp, D.M., Rinaldo, D., Halls, M.D., Zhang, J., and Friesner, R.A. (2013). Jaguar: A high-performance quantum chemistry software program with strengths in life and materials sciences. Int. J. Quantum Chem. *113*, 2110–2142. https://doi.org/10.1002/qua.24481.

53. Vanquelef, E., Simon, S., Marquant, G., Garcia, E., Klimerak, G., Delepine, J.C., Cieplak, P., and Dupradeau, F.Y. (2011). a web service for deriving RESP and ESP charges and building force field libraries for new molecules and molecular fragments. Nucleic Acids Res. *39*, W511–W517. https://doi.org/10.1093/nar/gkr288.

54. Nguyen, H., Roe, D.R., and Simmerling, C. (2013). Improved generalized born solvent model parameters for protein simulations. J. Chem. Theory Comput. *9*, 2020–2034. https://doi.org/10.1021/ct3010485.

55. Loncharich, R.J., Brooks, B.R., and Pastor, R.W. (1992). Langevin dynamics of peptides: the frictional dependence of isomerization rates of N-acetylalanyl-N'-methylamide. Biopolymers *32*, 523–535. https://doi.org/10.1002/bip.360320508.

56. Hopkins, C.W., Le Grand, S., Walker, R.C., and Roitberg, A.E. (2015). Long-Time-Step Molecular Dynamics through Hydrogen Mass Repartitioning. J. Chem. Theory Comput. *11*, 1864–1874. https://doi.org/10.1021/ct5010406.

57. Miller, B.R., McGee, T.D., Swails, J.M., Homeyer, N., Gohlke, H., and Roitberg, A.E. (2012). MMPBSA.py: An Efficient Program for End-State Free Energy Calculations. J. Chem. Theory Comput. *8*, 3314–3321. https://doi.org/10.1021/ct300418h.

58. Angers, S., Li, T., Yi, X., MacCoss, M.J., Moon, R.T., and Zheng, N. (2006). Molecular architecture and assembly of the DDB1-CUL4A ubiquitin ligase machinery. Nature *443*, 590–593. https://doi.org/10.1038/nature05175.

59. Schrödinger, L., and DeLano, W. (2020). PyMOL. http://www.pymol.org/pymol.

60. Plechanovová, A., Jaffray, E.G., Tatham, M.H., Naismith, J.H., and Hay, R.T. (2012). Structure of a RING E3 ligase and ubiquitin-loaded E2 primed for catalysis. Nature *489*, 115–120. https://doi.org/10.1038/nature11376.

61. Zhang, Q., Hossain, D.M.S., Nechaev, S., Kozlowska, A., Zhang, W., Liu, Y., Kowolik, C.M., Swiderski, P., Rossi, J.J., Forman, S., et al. (2013). TLR9-mediated siRNA delivery for targeting of normal and malignant human hematopoietic cells in vivo. Blood *121*, 1304–1315. https://doi.org/10.1182/blood-2012-07-442590.

62. Hossain, D.M.S., Dos Santos, C., Zhang, Q., Kozlowska, A., Liu, H., Gao, C., Moreira, D., Swiderski, P., Jozwiak, A., Kline, J., et al. (2014). Leukemia cell-targeted STAT3 silencing and TLR9 triggering generate systemic antitumor immunity. Blood *123*, 15–25. https://doi.org/10.1182/blood-2013-07-517987.